JOURNAL OF AIRCRAFT
Vol. 46, No. 1, January–February 2009

Optimal Placement of Piezoelectric Actuated Trailing-Edge Flaps for Helicopter Vibration Control

S. R. Viswamurthy* and Ranjan Ganguli†
Indian Institute of Science, Bangalore 560 012, India

DOI: 10.2514/1.38199

This study aims to determine the optimal locations for dual trailing-edge flaps on a helicopter blade in the presence of actuator hysteresis. An aeroelastic analysis based on a finite element approach in space and time is used in conjunction with an optimal control algorithm to determine the actuator control input for vibration minimization. The reduced hub-vibration level and the flap power are the two optimization indices considered in this study. The location of the flaps along the blade are the design variables. The hysteresis in the piezo-actuators is modeled using a dynamic hysteresis model based on an extension to the classical Preisach model. It is found that second-order polynomial response surfaces based on the central composite design of the theory of design of experiments describe both objectives adequately. Numerical studies for a four-bladed hingeless rotor show that both objectives are more sensitive to outboard flap location compared with inboard flap location. Optimization studies indicate that the dual-flap configuration for the least hub-vibration level is different from the configuration for the least flap power. The Pareto front between the two objectives is found to be discontinuous. However, a reasonable tradeoff configuration is obtained by careful inspection of the Pareto front. This configuration yields about a 70% reduction in hub-vibration levels from the baseline conditions at an advance ratio of 0.30, while requiring about 21% more flap power from the initial configuration of the optimization study.

Nomenclature

C_T	=	rotor thrust coefficient
c	=	blade chord
c_f	=	trailing-edge flap chord
EI_y	=	flap bending stiffness
EI_z	=	lag bending stiffness
F_x	=	vibratory hub longitudinal shear force
F_y	=	vibratory hub lateral shear force
F_z	=	vibratory hub vertical shear force
GJ	=	torsion stiffness
J	=	objective function
M_h	=	trailing-edge flap hinge moment
M_x	=	vibratory hub roll moment
M_y	=	vibratory hub pitch moment
M_z	=	vibratory hub yaw moment
m_f	=	trailing-edge flap mass per unit length
m_0	=	blade mass per unit length
P_f	=	power required by a single trailing-edge flap, averaged over one revolution
P_t	=	total actuation power required by all flaps on all rotor blades, averaged over one revolution
R	=	rotor radius
u	=	input to the hysteresis transducer/voltage applied to the piezostack, V
X_g^f	=	trailing-edge flap center of gravity (after hinge)
x_1, x_2	=	nondimensional location of the inboard and outboard flap, respectively
δ	=	output of the hysteresis transducer/flap deflection angle, deg
Γ	=	hysteresis operator
γ	=	lock number
μ	=	advance ratio/Preisach distribution function
μ_0, μ_1, μ_2	=	Preisach distribution functions for the dynamic hysteresis model
σ	=	blade solidity ratio
ψ	=	blade azimuth angle
Ω	=	rotor angular speed

Subscripts

St	=	steady component
Nc	=	Nth cosine harmonic
Ns	=	Nth sine harmonic

Superscript

$4p$	=	4/rev component

I. Introduction

HIGH vibration levels in helicopters lead to poor ride quality and passenger discomfort and reduce the fatigue life of critical components [1]. Reduction in airframe vibration is therefore of great importance to the rotorcraft industry. Early studies in this field suggested various passive methods to alleviate this problem [2]. In the last two decades, active approaches to control helicopter vibration have received considerable attention due to their relative advantages over the traditional passive methods [3–8]. Among the active approaches, the actively controlled flap (ACF) approach appears most feasible for full-scale implementation due to its conceptual simplicity and lower actuation power requirements [7,8]. Furthermore, the on-blade control surface is not in series with the primary flight control system and can be dealt with separately, thus reducing the difficulties of ensuring adequate airworthiness.

Several analytical and numerical studies have investigated the applications and advantages of the ACF approach. Milgram et al. presented a comprehensive study of vibration reduction in helicopters using an actively controlled trailing-edge flap [9]. Spencer et al. studied the possibility of employing an adaptive neurocontroller to suppress vibration using a piezo-actuated trailing-

Presented as Paper 1791 at the 16th AIAA/ASME/AHS Adaptive Structures Conference, Schaumburg, Illinois, 4 July–4 October 2008; received 22 April 2008; revision received 26 September 2008; accepted for publication 9 October 2008.

*Graduate Student; currently Postdoctoral Fellow, Seoul National University, Korea; viswamurthy@gmail.com.

†Associate Professor, Department of Aerospace Engineering; ganguli@aero.iisc.ernet.in. Associate Fellow AIAA.

edge flap [10]. Myrtle and Friedmann combined the rational function approximation approach with a free-wake model to determine the aerodynamic loads under attached flow conditions [11]. Wind-tunnel tests on scaled rotor models with on-blade active flaps confirm the promise shown by this approach [12,13]. Recently, Eurocopter conducted a series of successful flight tests of a modified BK117 helicopter with piezo-actuated trailing-edge flaps [14]. The active flap system performed well in the open-loop mode while the flaps were actuated between 2 and 5/rev frequencies. A reduction of up to 60–80% in 4/rev cabin vibrations at the pilot seat was achieved at a level forward speed of 100 kt.

On-blade trailing-edge flaps are typically moved at higher harmonics of the rotor rotational speed to reduce vibration in the fixed frame. Several approaches to actuate these flaps can be found in the literature: piezo-bimorph actuators [12,13], piezoelectric stack actuators [15], magnetostrictive actuators [16], induced shear tube actuators [17], to name a few. Among the various choices, piezoelectric stack actuators appear the most likely candidate for full-scale rotor applications due to their high energy density, bandwidth, actuation force, and low weight characteristics. However, a fundamental limitation of piezoceramic materials is their inherent nonlinearity and hysteresis. Most piezoceramic materials are fundamentally nonlinear in their response to an applied electric field, often exhibiting hysteresis between the electric field and displacement. Mechanical linkages designed to amplify the stroke of piezoelectric actuators tend to amplify this hysteresis effect. Not modeling hysteresis in the piezoelectric actuator often leads to loss of accuracy in open-loop control and affects system stability in closed-loop control [18,19]. Most studies involving active control of helicopter vibration using smart materials neglect the presence of actuator hysteresis. In a rare study addressing hysteresis effects, Kurdila et al. [20] derived a control methodology that accounts for the overall hysteresis in lead-zirconate-titanate actuated elevons. However, they represented the helicopter with a simple linear aeroelastic model, and the objective was not vibration control. Viswamurthy and Ganguli studied the effect of piezoelectric hysteresis on helicopter vibration control using a trailing-edge flap [21]. They used experimental data to develop a static hysteresis model for the actuator hysteresis. Their investigation also included extensive studies on a four-bladed hingeless rotor with single and multiharmonic control inputs to the active flap. They concluded that actuator hysteresis can be a crucial factor in determining the extent of vibration attenuation achieved in rotors with active flap systems. In another study, the same authors demonstrated that hysteresis compensation schemes can be employed to greatly improve the performance of the control algorithm in the presence of actuator hysteresis [22]. However, one drawback of the approach followed in [22] was the limited applicability of compensation schemes to only actuators with "static" hysteresis properties. This issue was addressed in a recent study by Viswamurthy et al., in which they extended the static model to characterize actuators with "dynamic" hysteresis [23]. It was found that dynamic hysteresis effects are important and need to be accounted for in the development of the controller.

Some recent studies have demonstrated the flexibility of multiple-flap configurations and their advantage over single trailing-edge flap configurations [24,25]. In general, multiple flaps can effectively excite the higher natural modes of the rotor blade by operating out of phase with respect to each other [26]. This property of the multiple-flap configuration gives an element of flexibility and effectiveness to its operation while also providing redundancy in the active flap system. Few studies have used a rigorous approach for the optimal placement of flaps to maximize the benefits of the active flap system. In one such study, Viswamurthy and Ganguli adopted an optimization approach for the spanwise placement of flaps in a dual-flap configuration to maximize the benefit of vibration reduction while minimizing flap power [27]. They used a polynomial response surface to approximate the vibration and flap-power objectives in terms of the location of the inboard and outboard flaps. This approach decoupled the aeroelastic control problem from the optimal flap placement problem while also drastically reducing the computational time of the optimization process. However, it must be mentioned that several other studies ignored the presence of hysteresis in the trailing-edge flap actuators [24–27].

In the present study, a response-surface-based optimization approach is followed to identify the best configuration of dual trailing-edge flaps that minimizes rotor hub vibrations in the presence of actuator dynamic hysteresis. The electrical power required to drive the piezostack actuators is typically transmitted from the nonrotating frame to the rotating frame through slip rings. It is therefore desirable to keep the trailing-edge flap-power requirements to a minimum. The hub-vibration level and flap actuation power are two conflicting objectives. An attempt to minimize one objective almost always leads to an increase in the other. Therefore, a multi-objective optimization approach is followed in this study. The integration of a high-fidelity, computationally intensive rotorcraft aeroelastic code with an optimization routine typically leads to an enormous computational challenge. This problem can be overcome by developing an inexpensive surrogate model, or metamodel, of the high-fidelity aeroelastic analysis [28,29]. The response-surface methodology is one such metamodeling technique and is used in this study [30].

II. Actuator Hysteresis Model

Hysteresis in ferromagnetic materials has been studied for a long time. In an early study, Preisach proposed a hysteresis model for magnetic hysteresis based on some hypotheses concerning the physical mechanisms of magnetization. This model, later referred to as the classical Preisach model (CPM), is popular due to its simplicity and is widely used in literature [18,19]. Krasnoselskii separated Preisach's model from its physical meaning and represented it in a pure mathematical form that is similar to a spectral resolution of operators [31]. As a result, this model can now be used for the mathematical description of hysteresis of any physical nature. The Preisach model has several appealing features, including its ability to model complex hysteresis types, a well-defined identification algorithm, and a convenient numerical simulation form [32]. The CPM can be represented in the following mathematical form:

$$\delta(\psi) = \Gamma u(\psi) = \iint_{\alpha \geq \beta} \mu(\alpha, \beta) \hat{\gamma}_{\alpha\beta}[u(\psi)] \, \mathrm{d}\alpha \, \mathrm{d}\beta \tag{1}$$

where $\hat{\gamma}_{\alpha\beta}$ is the elemental hysteresis operator shown in Fig. 1 and α and β are its switching values. The Preisach distribution function, $\mu(\alpha, \beta)$, is a characteristic of the piezoelectric actuator. If the distribution function (sometimes referred to as the Preisach measure or, simply, the weighting function) is known, then Eq. (1) can be solved directly by integration. If the function $\mu(\alpha, \beta)$ is not known explicitly, then experimental data are needed to estimate the Preisach distribution function using geometric interpretation [32].

The CPM, though widely used, has some limitations. One shortcoming is its ability to model only static hysteresis phenomena. The term static means that the system output predicted by CPM depends only on the current input and past extremum values of input, whereas the speed of the input variation has no influence on the output [32]. This inhibits the use of CPM to model systems that exhibit rate-dependent hysteresis phenomena. Mayergoyz [33] was the first to propose an extension to the CPM to model dynamic

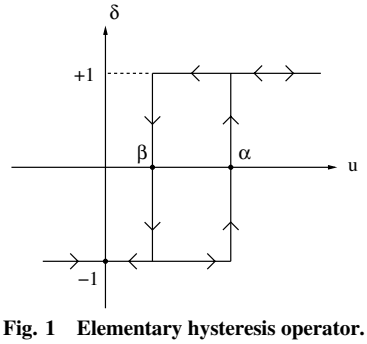

Fig. 1 Elementary hysteresis operator.

hysteresis. Mayergoyz suggested the relaxation of the "static property" of CPM by introducing a dependence of the Preisach distribution function on the rate of output variations, $\frac{d\delta}{d\psi}$. The dynamic hysteresis models is then written as

$$\delta(\psi) = \iint_{\alpha \geq \beta} \mu\left(\alpha, \beta, \frac{d\delta}{d\psi}\right) \hat{\gamma}_{\alpha\beta}[u(\psi)]\, d\alpha\, d\beta \tag{2}$$

In this model, the Preisach measure, μ, is dependent on the unknown output rate ($\frac{d\delta}{d\psi}$). This difficulty is overcome by using the Taylor series expansion for μ with respect to ($\frac{d\delta}{d\psi}$):

$$\mu\left(\alpha, \beta, \frac{d\delta}{d\psi}\right) = \mu_0(\alpha, \beta) + \frac{d\delta}{d\psi}\mu_1(\alpha, \beta) + \frac{d^2\delta}{d\psi^2}\mu_2(\alpha, \beta) + \cdots \tag{3}$$

In the current study, only the first three terms on the right-hand side of Eq. (3) are retained. Substituting this relation into Eq. (2) gives the following dynamic hysteresis model:

$$\begin{aligned}\delta(\psi) = &\iint_{\alpha \geq \beta} \mu_0(\alpha, \beta)\hat{\gamma}_{\alpha\beta}[u(\psi)]\, d\alpha\, d\beta \\ &+ \frac{d\delta}{d\psi}\iint_{\alpha \geq \beta} \mu_1(\alpha, \beta)\hat{\gamma}_{\alpha\beta}[u(\psi)]\, d\alpha\, d\beta \\ &+ \frac{d^2\delta}{d\psi^2}\iint_{\alpha \geq \beta} \mu_2(\alpha, \beta)\hat{\gamma}_{\alpha\beta}[u(\psi)]\, d\alpha\, d\beta\end{aligned} \tag{4}$$

It is obvious that, in the case of very slow output variations, this dynamic model reduces to the classical Preisach model. The function μ_0 is, in fact, the Preisach measure of the static Preisach model and can be estimated using known methods [32]. In the current study, the function μ_0 is estimated based on the quasi-static response of an APA500L actuator from CEDRAT Technologies. The other two unknown measures, μ_1 and μ_2, are estimated by a least-squares method using experimental data of the actuator at higher operational frequencies [23].

III. Aeroelastic Analysis of a Helicopter

A. Structural Model

The structural model of the helicopter is composed of a nonlinear model of elastic rotor blades coupled with a rigid fuselage model. Each rotor blade is modeled as a slender beam undergoing in-plane bending, out-of-plane bending, elastic twist, and axial deflection. A second-order, nonlinear, moderate deflection theory proposed by Hodges and Dowell [34] is used. The trailing-edge flaps are assumed to be an integral part of the blade, and the flap hinge is assumed to coincide with its leading edge. The flap hinges are assumed to be rigid in all directions except about the hinge axis, thereby allowing only pure rotation of the flap in the plane of the blade cross section. It is also assumed that the flaps do not contribute to the stiffness of the rotor blade and only influence the behavior of the blade through their contribution to the blade spanwise aerodynamic and inertial loading. Moreover, the flaps are not aerodynamically balanced.

B. Aerodynamic Model

The quasi-steady component of the aerodynamic loads are calculated based on the table lookup approach from airfoil static data. The reverse flow is modeled by considering the chordwise shift in the aerodynamic center location [35]. The aerodynamic forces and moments acting on the blade section are calculated for unsteady profile and trailing-edge flap motion in the forward flight condition. The attached flow formulation is based on the indicial response method in which the response is calculated from a finite difference approximation to Duhamel's integral [36]. Compressibility effects are implicitly included in the indicial response functions. The additional aerodynamic loads caused by trailing-edge flap motion are calculated using a time domain unsteady aerodynamic model proposed by Hariharan and Leishman [37]. A free-wake model is used to determine the induced inflow distribution over the rotor disk [38]. Further details about the aerodynamic modeling are available in [21].

C. Formulation and Solution Procedure

The aeroelastic formulation in this study is based on the Hamilton's principle:

$$\int_{\psi_1}^{\psi_2} (\delta U - \delta T - \delta W)\, d\psi = 0 \tag{5}$$

where δU, δT, and δW are the virtual strain energy, kinetic energy, and work, respectively.

Finite element methodology is used to discretize the governing equations of motion. The rotor blade is discretized into a number of beam finite elements, and each finite element has 15 degrees of freedom [35]. The spatial functionality is removed by the finite element discretization, thereby converting the set of partial differential equations into a set of ordinary differential equations. To reduce the computational cost, the finite element equations in terms of the nodal displacements are transformed into modal space. Four flap, four lag, and two torsion modes are used in this study. The blade response is solved in modal space using a finite element in time approach [39]. A coupled trim/aeroelastic solution procedure is carried out to simultaneously solve for the blade nonlinear steady response, pilot input trim controls, and vehicle orientation. The vehicle trim is solved while including the trailing-edge flap inputs. Steady and vibratory components of the rotating frame blade loads are calculated using a force summation method. In this approach, the blade inertia and aerodynamic forces are integrated directly over the length of the blade. Fixed-frame hub loads are calculated by summing the contributions of individual blades at the root. The hub forces and moments are nondimensionalized with respect to $m_0\Omega^2R^2$ and $m_0\Omega^2R^3$, respectively. Additional details of the aeroelastic analysis can be found in Viswamurthy and Ganguli [24] and Bir et al. [35].

The mean power required by a trailing-edge flap (single blade) is obtained by integrating the product of its hinge moment and flap deflection rate over one rotor revolution:

$$P_f = -\frac{1}{2\pi}\int_0^{2\pi} M_h\dot{\delta}\, d\psi \tag{6}$$

The flap power required may change sign over some portions of the azimuth. As the actuator will generally not be able to transfer this power back to the flap actuation power supply, the negative power is neglected. Therefore, the mean actuation power for the complete flap system for a N_b-bladed rotor with N_f flaps in each rotor blade can be written as follows:

$$P_t = \frac{N_b}{2\pi}\sum_{i=1}^{N_f}\int_0^{2\pi} \max\left(-M_{hi}\frac{d\delta_i}{d\psi}, 0\right) d\psi \tag{7}$$

IV. Flap Control Algorithm

In the current investigation, a hingeless rotor with four identical blades is considered. For such a rotor, the hub dynamic loads in the fixed frame are dominated by the 4/rev component. In steady forward flight, the helicopter rotor system can be assumed to be periodic in time. This periodic nature of the system allows us to transform the control problem from the time domain to the frequency domain [40]. Actuation of the trailing-edge flap(s) at 2, 3, 4, and 5/rev harmonics in the rotating frame is the best way to alleviate the 4/rev hub loads in the fixed frame. The 2/rev excitation of the blade pitch is beneficial for reducing blade-vortex interaction induced vibration and noise whereas the 3, 4, and 5/rev harmonics are well known to affect the 4/rev fixed system loads [14]. In any case, if the 2/rev input is not beneficial for the flight condition considered in this study, the control algorithm will drive the 2/rev inputs to zero. The control algorithm used in this study is based on the minimization of an objective function that is a quadratic function of hub vibratory loads and

control input magnitudes. This algorithm is a modified version of the original algorithm proposed by Johnson [40]. In this study, the control input is the applied actuator voltage instead of the flap deflection itself. Each rotor blade is assumed to have two trailing-edge flaps. A nonzero steady component of flap motion can affect pilot trim control angles. This is prevented by giving a dc bias to the stack actuator. This dc bias is adjusted so as to obtain a flap motion with zero steady component. The total voltage applied to the piezostack driving the jth flap is then given by

$$u^j(\psi) = u^j_{\text{st}} + \sum_{N=2}^{5}[u^j_{Nc}\cos(N\psi) + u^j_{Ns}\sin(N\psi)], \qquad j = 1, 2 \tag{8}$$

At the ith control step, the objective function for optimal control is given by

$$J(\mathbf{Z}_i, \mathbf{u}^1_i, \mathbf{u}^2_i) = \mathbf{Z}^T_i \mathbf{W}_Z \mathbf{Z}_i + \sum_{j=1}^{2} \beta^j \mathbf{u}^{jT}_i \mathbf{u}^j_i \tag{9}$$

where $\mathbf{Z}_i$ is the vibratory hub load vector at the ith control step containing the 4Ω sine and cosine harmonics (three hub shears and three hub moments), and $\mathbf{u}^j_i$ is the control input vector containing the cosine and sine higher harmonics of the jth flap at the ith control step. Because u^j_{st} is not an independent parameter, it is not included in the vector of control input harmonics $\mathbf{u}^j_i$. The diagonal matrix $\mathbf{W}_Z$ is a weighting matrix for hub vibratory loads. The first term in Eq. (9) is a scalar quantity that is purely related to the magnitude of the hub vibratory loads and is a measure of hub vibration. The nondimensional weighting parameters β^j can be changed to establish the relative importance of hub loads vs flap motions in the objective function. When $\beta^j = 0$, the controller tries to minimize hub loads without regard to the motion of the jth trailing-edge flap. As β^j is increased toward unity, the controller attempts to reduce the motion of the jth trailing-edge flap to zero.

$$\mathbf{Z}_i = \begin{bmatrix} F^{4p}_x & F^{4p}_y & F^{4p}_z & M^{4p}_x & M^{4p}_y & M^{4p}_z \end{bmatrix}^T \tag{10}$$

$$\mathbf{u}^j_i = \begin{bmatrix} u^j_{2c} & u^j_{2s} & u^j_{3c} & u^j_{3s} & u^j_{4c} & u^j_{4s} & u^j_{5c} & u^j_{5s} \end{bmatrix}^T, \qquad j = 1, 2$$

$$\mathbf{W}_Z = \left(1 - \sum_{j=1}^{2} \beta^j\right)\mathbf{I}_{6X6} \qquad \sum_{j=1}^{2} \beta^j \le 1 \tag{11}$$

The subscript i in Eqs. (9) and (10) refers to the ith control step, reflecting the discrete-time nature of the control. The time interval between each control step must be sufficient to allow the system to return to the steady state so that the vibration level can be measured accurately. A linear, frequency domain representation of helicopter response to control input is used in the minimization of the objective function. In this study, the "feedback form of the global controller" proposed by Millott and Friedmann is implemented [41]. Linearizing the system about the current control inputs using the Taylor series expansion gives

$$\mathbf{Z}_i = \mathbf{Z}_{i-1} + \sum_{j=1}^{2} \mathbf{T}^j_0(\mathbf{u}^j_i - \mathbf{u}^j_{i-1}) \tag{12}$$

where $\mathbf{T}^j_0$ is the transfer matrix that relates the system response to the motion of the jth trailing-edge flap. This transfer matrix is assumed to be constant over the entire range of the control input and, hence, is calculated only once by perturbing the control harmonics individually around zero control inputs. Equation (12) is substituted in Eq. (9), and the optimal controller is obtained by applying the following optimality criteria:

$$\frac{\partial J}{\partial \mathbf{u}^j_i} = 0, \qquad j = 1, 2 \tag{13}$$

The global controller used in this paper is robust to small changes in several plant parameters [42]. Viswamurthy and Ganguli [42] have shown that, though a local controller gives better results in some situations, the advantage is not enough to compensate for the enormous computer time required by the local controller.

V. Optimization Problem

The primary objective of this study as stated in Sec. I is to determine an optimal configuration of a dual trailing-edge flap system to achieve a maximum reduction in hub-vibration levels while attempting to minimize flap actuation power. For a given dual-flap configuration, the hub-vibration cost functional (denoted by J^*_v) is obtained by evaluating the first term on the right-hand side of Eq. (9) after solving Eq. (13). This value is an estimate of the reduced hub-vibration levels achievable with the flap configuration considered. The flap-power cost functional can then be evaluated using Eq. (7). The optimization problem then becomes the minimization of the two cost functionals, J^*_v and P_t, in the presence of actuator hysteresis, with the locations of the inboard and outboard flaps serving as the unknown design variables. In this study, the cost functionals, J^*_v and P_t, are normalized with respect to their corresponding values at a chosen initial configuration (Fig. 2). These normalized values are denoted by F_v and F_p, respectively. The optimization problem is then mathematically posed as

$$\text{minimize } \{F_v, F_p\} \text{ subject to: } x_{1-\text{lower}} \le x_1 \le x_{1-\text{upper}}$$
$$x_{2-\text{lower}} \le x_2 \le x_{2-\text{upper}} \tag{14}$$

The nondimensional flap locations, x_1 and x_2, are constrained by placing move limits (Fig. 2). The lower limit on the inboard flap prevents it from operating in a comparatively low dynamic pressure region in which it will be less effective. The outboard flap is prevented from being placed too near the blade tip to avoid the three-dimensional flow and blade tip-loss effects. The two objectives, F_v and F_p, are usually conflicting in nature, and it is unlikely that both objectives would be minimized by the same choice of design variables. This problem falls under the domain of multi-objective optimization. The nature of the tradeoff between the two objectives (F_v and F_p) depends on the shape of the Pareto curve/surface. A solution to a multi-objective optimization problem is said to be *Pareto optimal* if it is impossible to minimize any one objective without allowing an increase in one or more of the other objectives.

A standard method of finding a Pareto point involves the minimization of a scalar objective function obtained by combining the various objectives. Typically, the scalar objective is a positively weighted convex sum of the individual objectives. However, this method has some drawbacks. First, a uniform distribution of weighting parameters seldom yields a uniform distribution of points on the Pareto surface. Often, most points are found clustered in certain parts of the Pareto surface. Furthermore, only convex parts of the Pareto surface can be obtained using the method of minimizing convex combinations of the individual objectives [43].

Another drawback of the weighted function method is the issue of computational cost. Optimization has to be performed for different sets of weighting parameters to obtain a fair idea of the Pareto surface, which is computationally expensive when function evaluations involve complex problems such as helicopter aeroelasticity. For instance, each evaluation of F_v or F_p involves

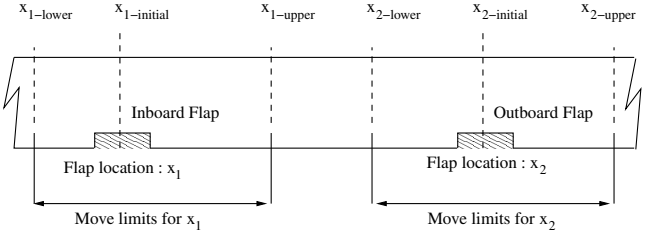

Fig. 2 Move limits of the dual-flap configuration.

calling the helicopter aeroelastic analysis 17 times (16 to evaluate the transfer matrix, $\mathbf{T}$, and once to determine the hub loads due to optimal control input, $\mathbf{Z}^*$). Each call to the aeroelastic analysis takes about 170 s of CPU time on a 256MB RAM Pentium-4 computer. This translates to 48 min of CPU time for one function evaluation of F_v or F_p. This prohibits the use of conventional optimization techniques to determine the optimal location of trailing-edge flaps. Response-surface approximations provide a solution to this problem by decoupling the optimization problem from the aeroelastic analysis. Once an approximate model is constructed, the optimum solution can be determined easily because the response surfaces are typically polynomial expressions.

A. Response-Surface Methodology

Response-surface methodology (RSM) provides an approximate relationship between the response of a system and its inputs. Typically smooth analytical functions, such as polynomials, are used for such approximations [44]. A lower-order smooth polynomial response surface removes the spurious minima/maxima while capturing the global trend of the response, thereby leading to a robust optimal design. For instance, a second-order polynomial response surface has the following form:

$$f(\mathbf{x}) = A_0 + \sum_{i=1}^{n} A_i x_i + \sum_{i=1}^{n} \sum_{j=1}^{i} A_{ij} x_i x_j \tag{15}$$

By appropriate choice of the regression coefficients (A_0, A_i, and A_{ij}) in Eq. (15), the function f can be made to approximately represent the actual response of the system around a point $\mathbf{x_0}$ in the design space. One method of determining the unknown regression coefficients is by comparing Eq. (15) with the second-order Taylor series expansion of the actual system response around $\mathbf{x_0}$. However, this method requires the gradient and Hessian information of the system response at $\mathbf{x_0}$. The determination of the gradient and Hessian for problems involving large computer programs such as helicopter aeroelastic analysis is a cumbersome and expensive process involving the method of finite differences. Also, in such cases, the choice of step size is critical in determining the gradient and Hessian accurately.

The unknown regression coefficients in Eq. (15) can also be determined using the method of curve fitting. A second-order polynomial response surface, as shown in Eq. (15), has $[n(n+1)/2 + n + 1]$ regression coefficients, where n is the number of system inputs. For instance, if $n = 2$, the second-order polynomial response surface with six regression coefficients can be written as

$$f(x_1, x_2) = A_0 + A_1 x_1 + A_2 x_2 + A_{11} x_1^2 + A_{12} x_1 x_2 + A_{22} x_2^2 \tag{16}$$

To determine the six regression coefficients uniquely, we need to evaluate the actual system response at six design points (called data points), at the least. A better fit can be constructed by evaluating the system response at more than six data points and using the method of least-square error to determine the coefficients. However, the computational cost to evaluate the system response at every additional data point limits the total number of response observations.

In the current study, a second-order response surface is used to approximate the functions F_v and F_p in terms of the independent variables x_1 and x_2 (nondimensional flap positions). Central composite design (CCD) is used for the optimal selection of data points to obtain a high-fidelity response-surface approximation [44]. This design consists of a center point encompassed by four axial and four factorial data points. Each independent variable is scaled such that each of the factorial points lies at the vertex of a unit square with its center at the central data point. Also, each axial point lies at a distance of $\alpha = 1.414$ from the center (Fig. 3). This choice of axial points ensures that any two design points that are equally distant from the center have an equally good prediction in response values. Once the system response is observed at the nine data points, the regression coefficients can be obtained using the method of least-squares error [44]. Formal methods of estimating the error in the response surfaces do exist. However, engineering judgement can often be used to account for the accuracy of the fitted model.

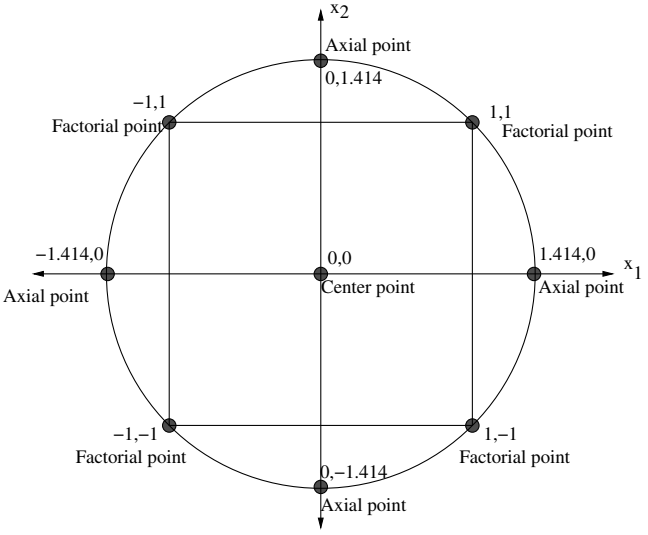

Fig. 3 Central composite design for two design variables.

VI. Numerical Results and Discussions

The properties of the soft-in-plane, uniform hingeless rotor considered in this study are shown in Table 1. The numerical studies in this investigation are conducted at a forward speed corresponding to an advance ratio of 0.30 and $C_T/\sigma = 0.07$. The use of a moderately low value of C_T/σ justifies the use of a linear airfoil model for the rotor blade air loads. Each flap spans 6% of the rotor blade span. The initial dual-flap configuration chosen to initiate the optimization process outlined in Sec. V is shown in Fig. 4. Table 2 provides the numerical values for the initial configuration and the move limits for the nondimensional variables x_1 and x_2.

A. Response-Surface Generation

The two objectives, F_v and F_p, defined in Sec. V are evaluated at the CCD data points using the aeroelastic analysis described in Sec. III. The response surfaces obtained by minimizing the error square are

$$\begin{aligned} F_v &= 1.000 + 0.0140x_1 - 0.0628x_2 + 0.0409x_1^2 \\ &\quad - 0.0096x_1x_2 - 0.1757x_2^2 \\ F_p &= 1.000 - 0.0172x_1 + 0.1676x_2 + 0.0598x_1^2 \\ &\quad + 0.0161x_1x_2 + 0.2428x_2^2 \end{aligned} \tag{17}$$

Table 1 Rotor blade and trailing-edge flap properties

Blade properties	
N_b	4
c/R	0.055
Solidity, σ	0.07
Lock number, γ	5.20
Blade pretwist	0.0
$EI_y/m_0\Omega^2R^4$	0.0108
$EI_z/m_0\Omega^2R^4$	0.0268
$GJ/m_0\Omega^2R^4$	0.00615
m_0, kg/m	6.46
Ω, rpm	383
R, m	4.94
Trailing-edge flap properties	
c_f/c	0.20
m_f/m_0	0.10
X_g^f/c_f	0.20

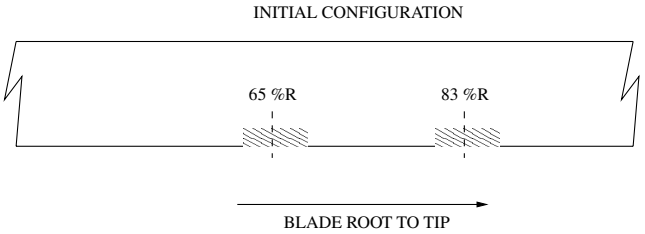

Fig. 4 Initial configuration chosen for the optimization routine.

Tables 3 and 4 show the comparison of response-surface prediction and aeroelastic analysis prediction at the nine data points for F_v and F_p, respectively. It is seen that the response surfaces approximate the actual objectives F_v and F_p fairly well (0–4% error). The mean error of the response surfaces predicting F_v and F_p is 0.01 and 0.03%, respectively. The standard deviation in both cases is 2.44 and 2.18%, respectively. It should be noted that, at each CCD data point, the control algorithm discussed in Sec. IV is employed to determine the optimal control input in the presence of actuator dynamic hysteresis. Figure 5 shows the variation in error with the response-surface predicted values for both objectives. The error in RSM prediction does not show any obvious trend and is distributed fairly randomly for both objectives.

B. Response-Surface Analysis

The stationary point of a response surface is found by setting its gradients to zero. For second-order polynomial response surfaces, this results in a set of linear equations that can be solved to a get unique solution for the stationary point. However, the second derivative information (Hessian matrix) is needed to determine whether the stationary point is a minima, a maxima, or a saddle point.

Table 2 Initial configuration and move limits

	Physical variable, R	Nondimensional value
$x_{1-\text{lower}}$	0.59	−1.414
$x_{1-\text{initial}}$	0.65	0
$x_{1-\text{upper}}$	0.71	1.414
$x_{2-\text{lower}}$	0.77	−1.414
$x_{2-\text{initial}}$	0.83	0
$x_{2-\text{upper}}$	0.89	1.414

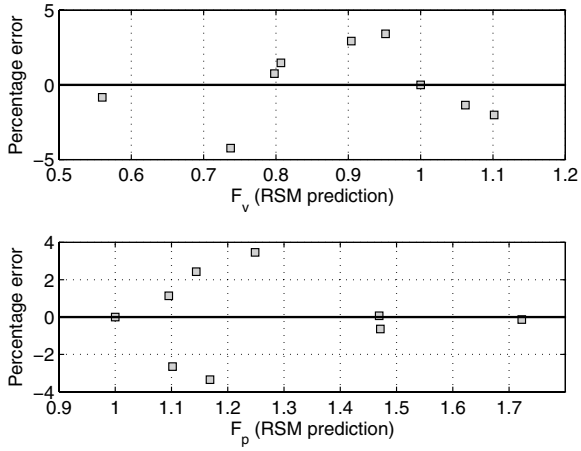

Fig. 5 Error vs RSM prediction.

Also, the stationary point is a feasible design only if it falls inside the move limits defined in Table 2.

1. *Vibration Minimization Only*

For the F_v response surface, the stationary point is found to be $x_1 = -0.192$ and $x_2 = -0.174$. This corresponds to inboard and outboard flap locations of 64.2 and 82.3%R, respectively. For this response surface, the eigenvalues of the Hessian matrix are $\lambda_1 = -0.352$ and $\lambda_2 = 0.082$. Because the eigenvalues are of different signs, the Hessian is indefinite and the stationary point is a saddle point. Figure 6 shows the variation of F_v with respect to the inboard and outboard flap locations. It is evident that the stationary point is indeed a saddle point. Figure 6 also suggests that F_v is more sensitive to the outboard flap location than the location of the inboard flap. Using an exhaustive search, the minimum value of F_v inside the move limits is found to be 0.560 corresponding to $x_1 = -0.007$ and $x_2 = 1.414$. This amounts to a 78% reduction in hub-vibration levels from the baseline (zero flap motion) conditions. The corresponding flap positions are 65 and 89% of the radial location from the blade root. This dual-flap configuration is designated as configuration A. This design corresponds to data point 2 in Tables 3 and 4. For this configuration, the F_p response surface predicts a value of 1.723. Configuration A is the best design for minimum hub-vibration levels in the presence of actuator hysteresis. However, this configuration

Table 3 RSM and aeroelastic analysis prediction of F_v at CCD data points

S. No.	x_1	x_2	Inboard flap location, R	Outboard flap location, R	F_v RSM prediction	F_v snalysis prediction	Error, %
1	0	0	0.65	0.83	1.0000	1.0000	0.00
2	0	1.414	0.65	0.89	0.5598	0.5645	−0.84
3	0	−1.414	0.65	0.77	0.7372	0.7699	−4.24
4	1.414	0	0.71	0.83	1.1016	1.1243	−2.02
5	−1.414	0	0.59	0.83	1.0619	1.0765	−1.36
6	−1	−1	0.61	0.79	0.9042	0.8785	2.93
7	−1	1	0.61	0.87	0.7979	0.7920	0.75
8	1	−1	0.69	0.79	0.9515	0.9201	3.42
9	1	1	0.69	0.87	0.8068	0.7951	1.47

Table 4 RSM and aeroelastic analysis prediction of F_p at CCD data points

S. No.	x_1	x_2	Inboard flap location, R	Outboard flap location, R	F_p RSM prediction	F_p analysis prediction	Error, %
1	0	0	0.65	0.83	1.0000	1.0000	0.00
2	0	1.414	0.65	0.89	1.7226	1.7248	−0.13
3	0	−1.414	0.65	0.77	1.2487	1.2070	3.46
4	1.414	0	0.71	0.83	1.0952	1.0829	1.14
5	−1.414	0	0.59	0.83	1.1439	1.1167	2.43
6	−1	−1	0.61	0.79	1.1684	1.2089	−3.35
7	-1	1	0.61	0.87	1.4712	1.4807	−0.64
8	1	−1	0.69	0.79	1.1017	1.1317	−2.65
9	1	1	0.69	0.87	1.4691	1.4680	0.07

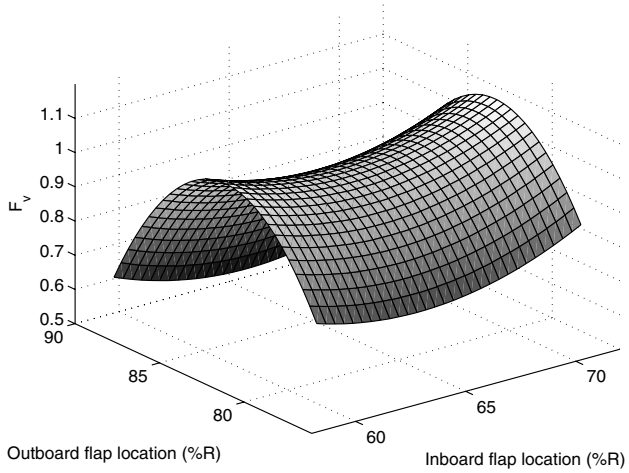

Fig. 6 Variation in F_v with trailing-edge flap positions in the presence of actuator dynamic hysteresis.

requires about 72% more flap power relative to the baseline design to achieve this superior performance. The shape of the response surface shown in Fig. 6 is similar to the response surface obtained in [27], in which the actuator hysteresis was neglected. Therefore, it is not surprising to see that configuration A is quite similar to the best configuration for minimum vibration in [27] (inboard flap: 63%R, outboard flap: 89%R).

2. Flap-Power Minimization Only

To obtain the flap configuration for least flap power, the stationary point of the F_p response surface has to be found. This is accomplished by setting the gradient of this response surface to zero. The solution thus obtained is $x_1 = 0.191$ and $x_2 = -0.352$. Because $-1.414 \leq x_1$ and $x_2 \leq 1.414$, this stationary point falls inside the allowable move limits. This corresponds to inboard and outboard flap locations of 65.8 and 81.5%R, respectively. This design point is quite near the initial design considered for response-surface studies and is denoted as configuration B. In this case, the eigenvalues of the Hessian matrix are $\lambda_1 = 0.119$ and $\lambda_2 = 0.486$. Because both eigenvalues are positive, the Hessian is positive definite; hence, the stationary point is a global minimum. Figure 7 shows the variation of F_p with respect to the trailing-edge flap locations. Again, it is seen that the objective F_p is quite sensitive to the outboard flap position. The global minimum point is clearly visible in Fig. 7. The response surface predicts $F_p = 0.969$ at this global minimum point. The aeroelastic analysis predicts a value of $F_p = 0.982$. The response-surface and aeroelastic analysis prediction of F_v at this design point is 1.005 and 0.986, respectively. This translates to about a 62% reduction in hub vibration from the baseline level. It is worth noting that the F_p response surface shown in Fig. 7 is fairly different from the response surface obtained in [27]. This difference can be directly attributed to the inclusion of actuator dynamic hysteresis in the present study.

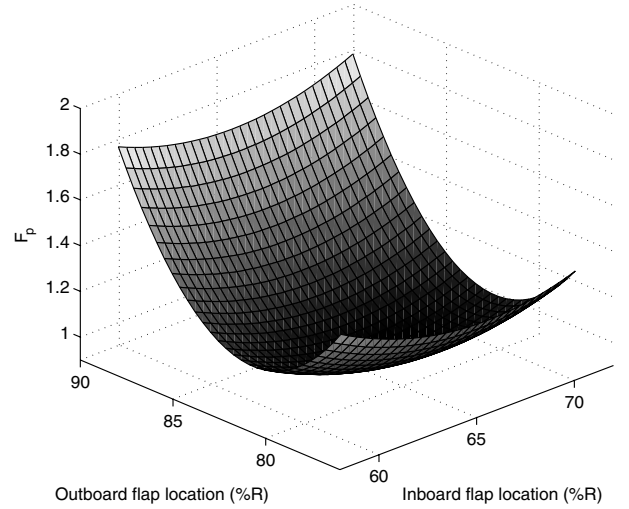

Fig. 7 Variation in F_p with trailing-edge flap positions in the presence of actuator dynamic hysteresis.

C. Vibration and Flap-Power Minimization

From the analysis of the two response surfaces in Figs. 6 and 7, it is evident that the best location for flaps for least hub-vibration levels and least flap power are different. The optimum inboard flap position for both objectives is about 65% radial location. For minimum hub-vibration levels, the outboard flap is required to be placed around 89% blade radial location. However, to achieve low flap-power consumption, the outboard flap needs to be positioned around 81.5% blade radial location. These two requirements are conflicting in nature. A tradeoff design solution is therefore sought that can lead to a substantial reduction in hub vibration while incurring a low penalty in terms of flap-power consumption. Although there are many ways to obtain such a design, a popular and easy way to approach this problem is by looking at the two response surfaces in the criterion space. This is accomplished by combining Figs. 6 and 7 and moving from the design space to the criterion space. Figure 8 shows the vibration level and flap power resulting from various design choices within the move limits. Because we have developed extremely computationally efficient polynomial response surfaces, an exhaustive search leads to all possible solutions for both objectives inside the defined move limits. As mentioned earlier, the design point $F_v = F_p = 1.0$ corresponds to the initial configuration shown in Fig. 4.

The Pareto surface between the two objectives F_v and F_p can be extracted from Fig. 8. Each point on the Pareto surface, or, in our case, the Pareto curve, represents a solution that has the following property: it is impossible to find a feasible solution that results in a lower value for one objective while the other objective is kept constant. The Pareto curve is shown in Fig. 9 and gives valuable information regarding the tradeoff characteristics between the two objectives. Also, it can be seen in Fig. 9 that the Pareto curve is discontinuous. Figure 9 also indicates the relative position of the initial configurations, configuration A and B, in the criterion space. As mentioned earlier, configuration B is quite close to the initial configuration and is the best choice for minimum flap-power consumption. Configuration A, on the other hand, is the best option for minimum hub-vibration levels but at the cost of higher flap power. These two configurations form the end points of the discontinuous Pareto curve. Configuration C, shown in Fig. 9, appears to be a good tradeoff design. It is expected to yield a reasonable combination of hub-vibration reduction and flap actuation power. The response-surface predicted values of F_v and F_p at this design point are 0.733 and 1.269, respectively. The actual

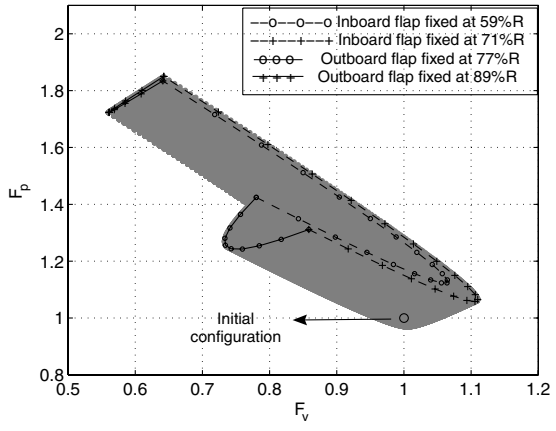

Fig. 8 F_p vs F_v for various design choices within the move limits.

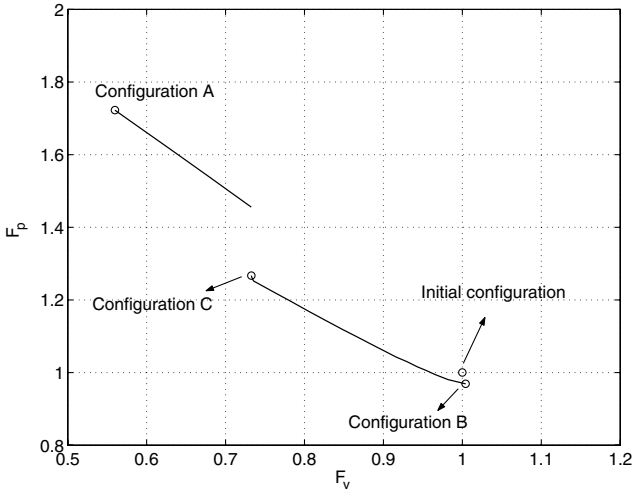

Fig. 9 Pareto surface between F_v and F_p.

values of the two objectives obtained by exciting the aeroelastic analysis for this configuration are 0.773 and 1.208, respectively. This translates to about a 70% reduction in hub vibration from baseline conditions (zero flap motion) while consuming about 21% more flap power relative to the initial design. This configuration is therefore chosen as the final design of this study.

Results from [27] indicate that, in the absence of actuator hysteresis, the Pareto curve between the two objectives becomes highly disjointed and lacks any intermediate tradeoff design solutions. In the current flap placement problem, the inclusion of an actuator hysteresis model has therefore resulted in more Pareto-optimal solutions and a feasible tradeoff design.

Configuration C, indicated in Fig. 9, corresponds to the nondimensional variables $x_1 = -0.334$ and $x_2 = -1.414$. The corresponding inboard and outboard flap positions are 63.6 and 77.0% of the radial location, respectively. The initial and final design configurations of the dual-flap system are shown in Fig. 10. Figure 11 shows the optimal control input for the final dual-flap configuration at a forward speed corresponding to an advance ratio of 0.30. It is seen that only the inboard flap operates near complete actuator

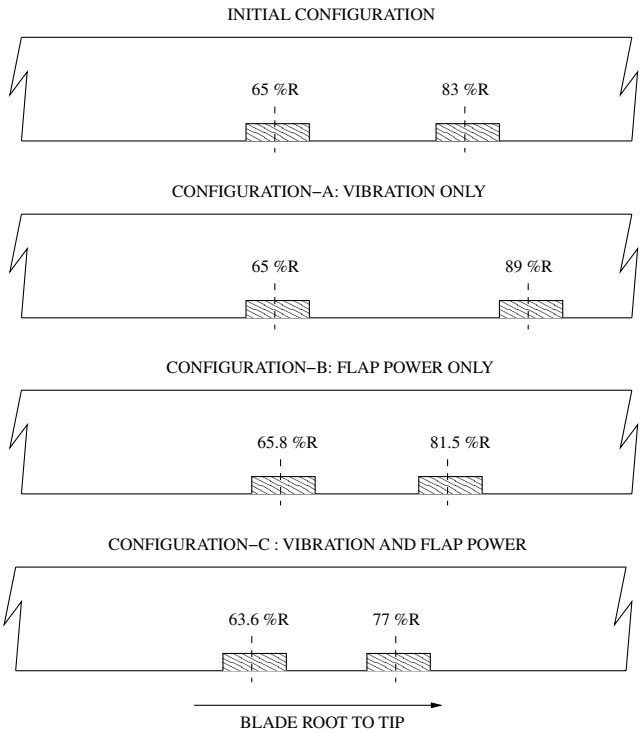

Fig. 10 Initial and other design configurations minimizing vibration, flap power, and both.

authority (−20 to +150 V). However, the control input to both flaps are nearly in phase. The flap motion resulting from the aforementioned optimal control input is shown in Fig. 12. The peak deflection of the inboard and outboard flaps are 2.65 and 1.81 deg, respectively. The hub-vibration levels are reduced by about 70% from the baseline (zero flap motion) levels. Figure 13 shows the reduction in individual 4/rev hub vibratory forces and moments. The longitudinal, lateral, and vertical 4/rev hub forces are reduced by about 23, 17, and 77% from their corresponding baseline values. The 4/rev rolling, pitching, and yawing hub moments are reduced by 22, 18, and 28%, respectively. We should point out that, for practical implementation, it may be useful to consider a point slightly away from and below configuration C. Such a point would be more robust, as a jump to the left will not make it nonoptimal owing to the discontinuity in the Pareto curve in Fig. 9.

D. Other Forward Speeds

The aforementioned studies were conducted at a speed corresponding to an advance ratio (μ) of 0.30. Figure 14 compares the performance of various design configurations at other forward speeds. Configuration A yields better vibration reduction than the initial configuration at all forward speeds but at the cost of higher flap-power consumption (about 33–111% higher). As expected, configuration B performs almost identically to the initial configuration in terms of both vibration reduction and flap-power consumption. This is because the flap locations in these two cases are

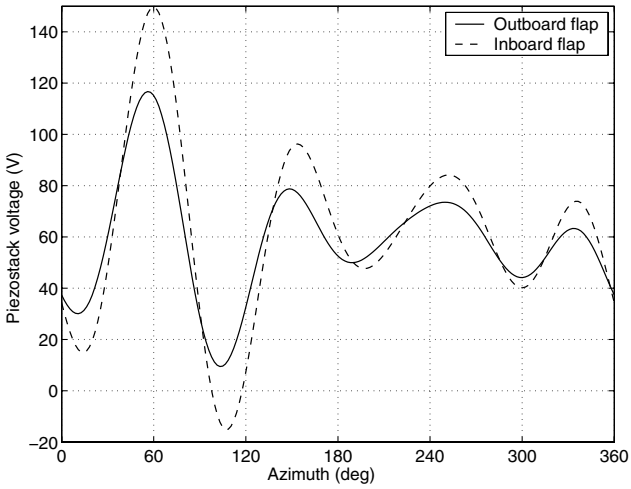

Fig. 11 Optimal control input; final configuration, $\mu = 0.30$.

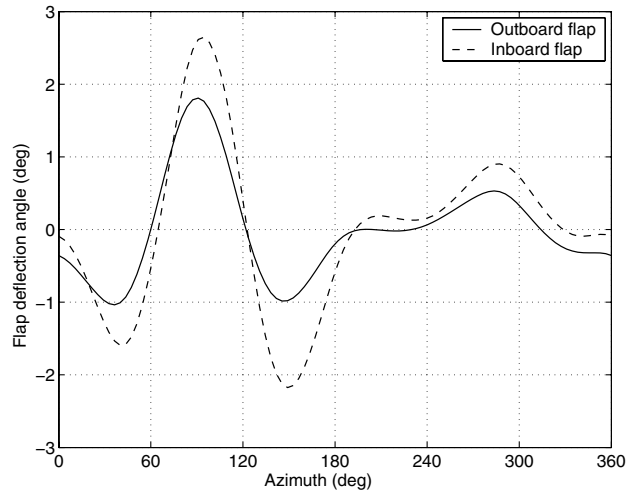

Fig. 12 Flap motion resulting from optimal control input; final configuration, $\mu = 0.30$.

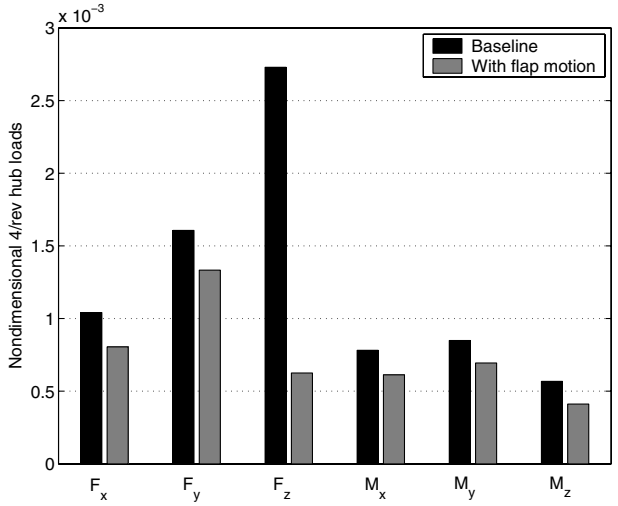

Fig. 13 Comparison of hub vibratory loads; final configuration, $\mu = 0.30$.

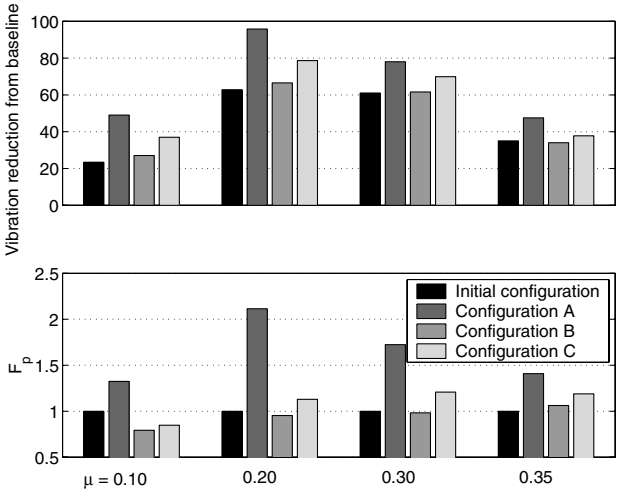

Fig. 14 Performance of various flap configurations at different forward speeds.

nearly the same. The final configuration (configuration C) is a good tradeoff design at other forward speeds too. It gives better reductions in hub-vibration levels compared with the initial configuration but with a very low additional flap-power penalty. It is therefore fair to say that the use of multi-objective optimization techniques in conjunction with response-surface methodology provides useful insight into the problem of the optimal placement of rotor trailing-edge flaps in the presence of actuator hysteresis. It is interesting to note that the actuator dynamic hysteresis not only has an effect on vibration reduction levels but also on optimal flap locations. The final dual-flap configuration chosen in this work provides a good tradeoff between the vibration objective and the flap-power objective at all forward speeds. We note some simplification and assumptions in this paper that can be addressed in future work. Aerodynamically balanced flaps for which the flap actuator hinge moment is eliminated can be considered. However, such balanced flaps may increase drag on the airfoil, which can result in an overall power penalty. The aerodynamic model could be refined with the use of nonlinear aerodynamics, which can be important for high-thrust conditions.

VII. Conclusions

In this study, the optimal position of dual trailing-edge flaps on a four-bladed, hingeless helicopter rotor in the presence of actuator dynamic hysteresis is sought. The performance criteria considered for the optimization study are the hub-vibration level and the power consumption of the trailing-edge flaps. The hysteresis in the piezo-actuators is modeled using a dynamic hysteresis model based on the classical Preisach model. A finite element approach is used to solve the coupled helicopter aeroelastic response and trim problem. The trailing-edge flaps are actuated at higher harmonics of the rotor rotation speed, and a frequency domain control algorithm is used to determine the flap control inputs. Second-order polynomial response surfaces are generated for the hub-vibration objective and flap-power objective using the central composite design. This approach decouples the optimization problem from the helicopter aeroelastic problem and greatly reduces the computational effort. For the specific rotor configuration used in this study and subject to the structural and aerodynamic assumptions used in the analysis, the following conclusions can be drawn:

1) The polynomial response surfaces obtained by using the central composite design offer valuable insight into the variation and sensitivity of the two objectives with respect to the location of the flaps.

2) Numerical results show that both hub-vibration level and flap-power objectives are more sensitive to the outboard flap location compared with the location of the inboard flap. The outboard flap is more effective in reducing hub-vibration levels due to its operation in a higher dynamic pressure region. For the same reason, the outboard flap encounters higher flap hinge moments leading to higher actuation power requirements.

3) To achieve minimum hub-vibration levels in the presence of actuator dynamic hysteresis, the inboard and outboard flaps need to be placed at 65 and 89% of the radial location, respectively (configuration A). This configuration is quite near the optimum configuration obtained in the absence of actuator hysteresis (63 and 89%R). Configuration A yields about a 78% reduction in hub vibration from baseline conditions while using about 72% more flap power compared with the initial configuration (65 and 83%R).

4) The Pareto curve between the two objectives, hub-vibration level and flap power, is discontinuous. The two configurations, A and B, form the end points of the discontinuous Pareto curve. However, unlike the case with no actuator hysteresis, the Pareto front in this study does contain some useful tradeoff design points that yield a reasonable reduction in hub vibration while consuming marginally more power than the initial configuration. The inclusion of actuator hysteresis has therefore resulted in more Pareto-optimal design points and a feasible tradeoff design.

5) A tradeoff dual-flap configuration is selected based on a careful examination of the Pareto front between the two objectives. In this final configuration, the inboard and outboard flaps are located at 63.6 and 77%R, respectively. This configuration yields a 70% reduction in hub vibration and requires about 2% more flap power compared with the initial configuration (for $\mu = 0.30$). This design point appears to be a good tradeoff between the two configurations, A and B, at all forward speeds.

References

[1] Ganguli, R., and Chopra, I., "Aeroelastic Optimization of a Helicopter Rotor to Minimize Vibration and Dynamics Stresses," *Journal of Aircraft*, Vol. 33, No. 4, 1996, pp. 808–815. doi:10.2514/3.47018

[2] Loewy, R., "Helicopter Vibrations: A Technological Perspective," *Journal of the American Helicopter Society*, Vol. 29, No. 4, 1984, pp. 4–30.

[3] Wood, E. R., Powers, R., Cline, J. H., and Hammond, C. E., "On Developing and Flight Testing a Higher Harmonic Control System," *Journal of the American Helicopter Society*, Vol. 30, No. 1, 1985, pp. 3–20.

[4] Thakkar, D., and Ganguli, R., "Dynamic Response of Rotating Beams with Piezoceramic Actuators," *Journal of Sound and Vibration*, Vol. 270, Nos. 4–5, 2004, pp. 729–753. doi:10.1016/S0022-460X(03)00189-5

[5] Thakkar, D., and Ganguli, R., "Use of Single Crystal and Soft Piezoceramics for Alleviation of Flow Separation Induced Vibration in Smart Helicopter Rotor," *Smart Material and Structures*, Vol. 15, No. 2, 2006, pp. 331–341. doi:10.1088/0964-1726/15/2/013

[6] Thakkar, D., and Ganguli, R., "Helicopter Vibration Reduction in Forward Flight with Induced Shear Based Piezoceramic Actuation," *Smart Material and Structures*, Vol. 30, No. 3, 1996, pp. 599–608.
[7] Friedmann, P. P., de Terlizzi, M., and Myrtle, T. F., "New Developments in Vibration Reduction with Actively Controlled Trailing Edge Flaps," *Mathematical and Computer Modelling*, Vol. 33, Nos. 10–11, 2001, pp. 1055–1083. doi:10.1016/S0895-7177(00)00300-9
[8] Wilbur, M. L., Mirick, P. H., Yeager, W. T., Langston, C. W., Cesnik, C. E. S., and Shin, S., "Vibratory Loads Reduction Testing of the NASA/Army/MIT Active Twist Rotor," *Journal of the American Helicopter Society*, Vol. 47, No. 2, 2002, pp. 123–133.
[9] Milgram, J. H., Chopra, I., and Straub, F. K., "Rotors with Trailing Edge Flaps: Analysis and Comparison with Experimental Data," *Journal of the American Helicopter Society*, Vol. 43, No. 4, 1998, pp. 319–332.
[10] Spencer, M. G., Sanner, R. M., and Chopra, I., "Adaptive Neurocontrol of Simulated Rotor Vibrations Using Trailing Edge Flaps," *Journal of Intelligent Material Systems and Structures*, Vol. 10, No. 11, 1999, pp. 855–871.
[11] Myrtle, T. F., and Friedmann, P. P., "Application of a New Compressible Time Domain Aerodynamic Model to Vibration Reduction in Helicopters Using an Actively Controlled Flap," *Journal of the American Helicopter Society*, Vol. 46, No. 1, 2001, pp. 32–43.
[12] Fulton, M. V., and Ormiston, R. A., "Hover Testing of a Small-Scale Rotor with On-Blade Elevons," *Journal of the American Helicopter Society*, Vol. 46, No. 2, 2001, pp. 96–106.
[13] Koratkar, N., and Chopra, I., "Wind Tunnel Testing of a Mach-Scaled Rotor Model with Trailing-Edge Flaps," *Smart Materials and Structures*, Vol. 10, No. 1, 2001, pp. 1–14. doi:10.1088/0964-1726/10/1/301
[14] Roth, D., Enenkl, B., and Dieterich, O., "Active Rotor Control by Flaps for Vibration Reduction-Full Scale Demonstrator and First Flight Test Results," *Proceedings of the 32nd European Rotorcraft Forum*, National Aerospace Laboratory, Amsterdam, Sept. 2006.
[15] Prechtl, E. F., and Hall, S. R., "Design of a High-Efficiency Discrete Servo-Flap Actuator for Helicopter Rotor Control," *Proceedings of the International Society for Optical Engineering*, Vol. 3041, June 1997, pp. 158–182. doi:10.1117/12.275645
[16] Fenn, R. C., Downer, J. R., Bushko, D. A., Gondhalekar, V., and Ham, N. D., "Terfenol-D Driven Flaps for Helicopter Vibration Reduction," *Smart Materials and Structures*, Vol. 5, No. 1, 1996, pp. 49–57. doi:10.1088/0964-1726/5/1/006
[17] Centolanza, L. R., Smith, E. C., and Munsky, B., "Induced-Shear Piezoelectric Actuators for Rotor Blade Trailing Edge Flaps," *Smart Materials and Structures*, Vol. 11, No. 1, 2002, pp. 24–35. doi:10.1088/0964-1726/11/1/303
[18] Hughes, D., and Wen, J. T., "Preisach Modeling of Piezoceramic and Shape Memory Alloy Hysteresis," *Smart Materials and Structures*, Vol. 6, No. 3, 1997, pp. 287–300. doi:10.1088/0964-1726/6/3/007
[19] Ge, P., and Jouaneh, M., "Modeling Hysteresis in Piezoceramic Actuators," *Precision Engineering*, Vol. 17, No. 3, July 1995, pp. 211–221. doi:10.1016/0141-6359(95)00002-U
[20] Kurdila, A. J., Li, J., Strganac, T., and Webb, G., "Nonlinear Control Methodologies for Hysteresis in PZT Actuated On-Blade Elevons," *Journal of Aerospace Engineering*, Vol. 16, No. 4, 2003, pp. 167–176. doi:10.1061/(ASCE)0893-1321(2003)16:4(167)
[21] Viswamurthy, S. R., and Ganguli, R., "Effect of Piezoelectric Hysteresis on Helicopter Vibration Control Using Trailing-Edge Flaps," *Journal of Guidance, Control, and Dynamics*, Vol. 29, No. 5, 2006, pp. 1201–1209. doi:10.2514/1.17655
[22] Viswamurthy, S. R., and Ganguli, R., "Modeling and Compensation of Piezoceramic Actuator Hysteresis for Helicopter Vibration Control," *Sensors and Actuators. A, Physical*, Vol. 135, No. 2, 2007, pp. 801–810. doi:10.1016/j.sna.2006.09.020
[23] Viswamurthy, S. R., Rao, A. K., and Ganguli, R., "Dynamic Hysteresis of Piezoceramic Stack Actuators Used in Helicopter Vibration Control: Experiments and Simulations," *Smart Materials and Structures*, Vol. 16, No. 4, 2007, pp. 1109–1119. doi:10.1088/0964-1726/16/4/020
[24] Viswamurthy, S. R., and Ganguli, R., "An Optimization Approach to Vibration Reduction in Helicopter Rotors with Multiple Active Trailing Edge Flaps," *Aerospace Science and Technology*, Vol. 8, No. 3, 2004, pp. 185–194. doi:10.1016/j.ast.2003.10.003
[25] Kim, J. S., Smith, E. C., and Wang, K. W., "Helicopter Vibration Suppression via Multiple Trailing Edge Flaps Controlled by Resonance Actuation System," *Proceedings of the 60th Annual Forum of the American Helicopter Society*, American Helicopter Society, Alexandria, VA, June 2004, pp. 1611–1622.
[26] Viswamurthy, S. R., and Ganguli, R., "Using Complete Authority of Multiple Active Trailing Edge Flaps for Helicopter Vibration Control," *Journal of Vibration and Control*, Vol. 14, No. 8, 2008, pp. 1175–1199. doi:10.1177/1077546307081323
[27] Viswamurthy, S. R., and Ganguli, R., "Optimal Placement of Trailing-Edge Flaps for Helicopter Vibration Reduction Using Response Surface Methods," *Engineering Optimization*, Vol. 39, No. 2, 2007, pp. 185–202. doi:10.1080/03052150601047123
[28] Barthelemy, J. F. M., and Haftka, R. T., "Approximation Concepts for Optimum Structural Design—A Review," *Structural Optimization*, Vol. 5, No. 3, 1993, pp. 129–144. doi:10.1007/BF01743349
[29] Murugan, S., and Ganguli, R., "Aeroelastic Stability Enhancement and Vibration Suppression in a Composite Helicopter Rotor," *Journal of Aircraft*, Vol. 42, No. 4, 2005, pp. 1013–1024. doi:10.2514/1.5652
[30] Roux, W. J., Stander, N., and Haftka, R. T., "Response Surface Approximation for Structural Optimization," *International Journal for Numerical Methods in Engineering*, Vol. 42, No. 3, 1998, pp. 517–534. doi:10.1002/(SICI)1097-0207(19980615)42:3<517::AID-NME370>3.0.CO;2-L
[31] Krasnoselskii, M. A., and Pokrovskii, A. V., *Systems with Hysteresis*, Springer, Berlin, 1983.
[32] Mayergoyz, I. D., "Mathematical Models of Hysteresis," *IEEE Transactions on Magnetics*, Vol. 22, No. 5, 1986, pp. 603–608. doi:10.1109/TMAG.1986.1064347
[33] Mayergoyz, I. D., "Dynamic Preisach Models of Hysteresis," *IEEE Transactions on Magnetics*, Vol. 24, No. 6, 1988, pp. 2925–2927. doi:10.1109/20.92290
[34] Hodges, D. H., and Dowell, E. H., "Nonlinear Equations of Motion for the Elastic Bending and Torsion of Twisted Nonuniform Rotor Blades," NASA TN D-7818, 1974.
[35] Bir, G., and Chopra, I., "University of Maryland Advanced Rotorcraft Code (UMARC) Theory Manual," University of Maryland Aerospace Engineering Rept. 92-02, 1992.
[36] Leishman, J. G., *Principles of Helicopter Aerodynamics*, Cambridge Univ. Press, New York, 2000.
[37] Hariharan, N., and Leishman, J. G., "Unsteady Aerodynamics of a Flapped Airfoil in Subsonic Flow by Indicial Concepts," *Journal of Aircraft*, Vol. 33, No. 5, 1996, pp. 855–868. doi:10.2514/3.47028
[38] Bagai, A., and Leishman, J. G., "Rotor Free-Wake Modeling Using a Pseudo-Implicit Technique Including Comparisons with Experimental Data," *Journal of the American Helicopter Society*, Vol. 40, No. 3, 1995, pp. 29–41.
[39] Borri, M., "Helicopter Rotor Dynamics by Finite Element Time Approximation," *Computers and Mathematics with Applications (1975-) / Computers & Mathematics with Applications*, Vol. 12A, No. 1, 1986, pp. 149–160. doi:10.1016/0898-1221(86)90092-1
[40] Johnson, W., "Self-Tuning Regulators for Multicyclic Control of Helicopter Vibrations," NASA TP-1996, March 1982.
[41] Millott, T. A., and Friedmann, P. P., "Vibration Reduction in Helicopter Rotors Using an Actively Controlled Partial Span Trailing Edge Flap Located on the Blade," NASA CR-4611, June 1994.
[42] Viswamurthy, S. R., and Ganguli, R., "Performance Sensitivity of Helicopter Global and Local Optimal Harmonic Vibration Controller," *Computers and Mathematics with Applications (1975-) / Computers & Mathematics with Applications*, Vol. 56, No. 10, 2008, pp. 2468–2480.
[43] Chen, W., Wiecek, M. M., and Zhang, J., "Quality Utility: A Compromise Programming Approach to Robust Design," *Journal of Mechanical Design*, Vol. 121, No. 2, 1999, pp. 179–187. doi:10.1115/1.2829440
[44] Myers, R. H., and Montgomery, D. C., *Response Surface Methodology-Process and Product Optimization Using Designed Experiments*, Wiley, New York, 1995.